Diffracting aperture based differential phase contrast for scanning X-ray microscopy

Burkhard Kaulich
Sincrotrone Trieste, X-ray microscopy section, S.S. 14 in Area Science Park, I-34012 Basovizza-Trieste, Italy

Francois Polack
Laboratoire pour l'Utilisation du Rayonnement Electronique (LURE), Campus d'Orsay, bat 209d, F-91405 Orsay Cedex, France

Ulrich Neuhaeusler, Jean Susini
ESRF, ID21 X-ray microscopy beamline, BP 220, F-38043 Grenoble Cedex, France

Enzo di Fabrizio
TASC-INFM, LILIT beamline, S.S. 14 in Area Science Park, I-34012 Basovizza-Trieste, Italy

Thomas Wilhein
University for Applied Sciences, RheinAhrCampus Remagen, Suedallee 2, D-53424 Remagen, Germany

Abstract: It is demonstrated that in a zone plate based scanning X-ray microscope, used to image low absorbing, heterogeneous matter at a mesoscopic scale, differential phase contrast (DPC) can be implemented without adding *any* additional optical component to the normal scheme of the microscope. The DPC mode is simply generated by an appropriate positioning and alignment of microscope apertures. Diffraction from the apertures produces a wave front with a non-uniform intensity. The signal recorded by a pinhole photo diode located in the intensity gradient is highly sensitive to phase changes introduced by the specimen to be recorded. The feasibility of this novel DPC technique was proven with the scanning X-ray microscope at the ID21 beamline of the European Synchrotron Radiation facility (ESRF) operated at 6 keV photon energy. We observe a differential phase contrast, similar to Nomarski's differential interference contrast for the light microscope, which results in a tremendous increase in image contrast of up to 20 % when imaging low absorbing specimen.

OCIS codes: (180.7460) X-ray microscopy, (180.5810), Scanning microscopy, (340.6720) Synchrotron radiation

References and Links

1. G. Schneider, "Cryo X-ray microscopy with high spatial resolution in amplitude and phase contrast," Ultramicroscopy **75**, 85-104 (1998)
2. U. Bonse and M. Hart, "An X-ray interferometer," Appl. Phys. Lett. **6**, 155-165 (1965)
3. G. Schmahl and D. Rudolph, "Proposal for a phase contrast X-ray microscope", in *X-ray Microscopy Instrumentation and Biological Applications*, P. C. Cheng and G. J. Jan, 231-238 (Springer, Berlin, 1987)
4. F. Polack, D. Joyeux, and J. Svaloš, "Applications of wavefront division interferometers in soft X-rays," Rev. Sci. Instrum. **66**, 2180-2183 (1995)
5. D. Joyeux, F. Polack, and D. Phallipou, "An interferometric determination of the refractive part of optical constants for carbon and silver across soft X-ray absorption edges," Rev. Sci. Instrum. **70**, 2921-2926 (1999)
6. G. Morrison, and B. Niemann, "Differential phase contrast X-ray microscopy," in *X-ray microscopy and Spectromicroscopy*, J. Thieme, G. Schmahl, D. Rudolph, and E. Umbach, I-95 - I-105 (Springer, Berlin, 1998)
7. H. N. Chapman, C. Jacobsen, and S. Williams, "Applications of a CCD detector in scanning-transmission X-ray microscopy," Rev. Sci. Instrum. **66**, 1332-1334 (1995)

#1552 - $15.00 US Received August 09, 2002; Revised September 27, 2002

8. T. Wilhein, B. Kaulich, E. Di Fabrizio, F. Romanato, S. Cabrini, and J. Susini, "Differential interference contrast X-ray microscopy with submicron resolution," Appl. Phys. Lett. **78**, 2082-2084 (2001)
9. B. Kaulich, T. Wilhein, E. Di Fabrizio, F. Romanato, M. Altissimo, S. Cabrini, B. Fayard, and J. Susini, "Differential interference contrast X-ray microscopy with twin zone plates," J. Opt. Soc. Am **A 19**, 797-806 (2002)
10. R.Barrett, B. Kaulich, M. Salome, and J. Susini, "Current status of the scanning X-ray microscope at the ESRF," AIP Conf. Proc. **507**, 458-463 (2000)
11. J. Susini, R. Barrett, B. Kaulich, S. Oestreich, and M. Salomé, "The X-ray microscopy facility at the ESRF: A status report," AIP Conf. Proc. **507**, 19-26 (2000)
12. E. Di Fabrizio, F. Romanato, M. Gentili, S. Cabrini, B. Kaulich, J. Susini, and R. Barrett, "High-efficiency multilevel zone plates for keV X-rays," Nature **401**, 895-898 (1999)
13. E.M. Waddell and J.N. Chapman, "Linear imaging of strong phase objects using asymmetrical detectors in STEM," Optik **54**, 83-96 (1979)

1. Introduction

Since the early development of microscopes for X-rays, it became rapidly obvious that phase sensitive techniques using the imaginary part of the refractive index should be preferred absorption based methods because (i) materials consisting of low Z-elements, especially organic matter have a low absorption, and (ii) it is predicted by several theoretical models that a lower radiation dose is applied to the specimen at similar or higher image contrast [1].

Phase sensitive techniques were introduced to X-rays by Bonse and Hart, who invented X-ray interferometry based on a double crystal in Laue geometry [2]. Phase sensitive techniques for sub-micron X-ray microscopy had to wait several decades for the development of higher generation X-ray sources and appropriate X-ray optics. Due to the complementarity of full-field imaging and scanning type microscopes, their X-ray source and detection requirements, different techniques have been developed in the past. Schmahl, Rudolph et al. proposed and proved a Zernike type phase contrast setup for full-field imaging type or transmission X-ray microscopy (TXM) [3]. Due to the versatility of detection modes in scanning X-ray microscopes (SXM), several phase techniques were developed independently for this type of X-ray microscope. Joyeux et al. performed experiments on Young type slit setups [4,5]. Morrison et al. and Chapman et al. used configured detectors or CCD cameras to extract absorption, phase contrast and dark-field images simultaneously [6,7]. Recently, a differential interference contrast technique similar to Nomarski interference contrast based on twin zone plates for X-rays was investigated, with the advantage of being applicable for both, SXM and TXM [8,9].

It is worth noting that the above techniques are of differential type, and therefore sensitive to the gradient of imaginary part of the transmission factor. Though very low frequency contents is not imaged in DPC mode, it has compared to Zernike phase contrast the advantage that artifact halos due to the finite extension of the phase plate are avoided. We describe here a setup for DPC in conventional zone plate (ZP) based SXM, which does not need any additional optical component and makes use only of the apertures already needed by the optical scheme of a standard SXM

2. Method and experimental description

In the experiment performed with the SXM [10] at the ID21 X-ray microscopy beamline [11] of the ESRF (see Fig. 1), X-ray light from an U42 undulator operated at 6 keV photon energy is monochromatized by a Si <111> double crystal monochromator. A ZP made of Au with an outermost zone width of 200 nm, a diameter of 69.7 µm and a focal length of 67.5 mm at 6 keV [12] demagnifies the source in 53 m distance to a diffraction limited micro-spot, across which the sample is raster scanned. Due to the fact that ZPs as diffractive optics have an infinite number of diffraction orders and foci, an order-sorting aperture is introduced into the optical scheme to eliminate other diffraction orders than the +1. order used for imaging. A central stop aperture is additionally needed to block zero order passing through ZP and OSA.

#1552 - $15.00 US Received August 09, 2002; Revised September 27, 2002

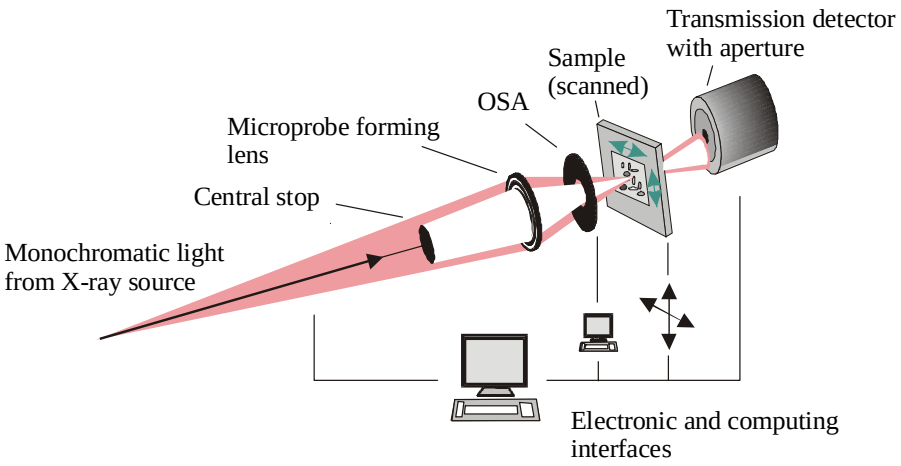

Fig. 1: Optical scheme of a scanning X-ray microscope operated in differential interference contrast (DPC) mode: The specimen is raster scanned across a microprobe formed by a coherently illuminated zone plate (ZP). Order sorting aperture (OSA) and central stop aperture eliminate spurious diffraction orders of the ZP only +1. order is used for imaging. Diffraction from both apertures modulates the wavefront. A detector shaped with a pinhole aperture is highly sensitive to phase slopes in the specimen and movements of fringes in the modulated wave front.

Both apertures diffract and lead to a complex wave front modulation in the far field beyond the object plane where the detector is located. A shaped detector positioned on a slope of the diffraction fringe is highly sensitive to fringe movements introduced by phase changes of the sample. In the reported experiment, an Au central stop with 40 µm in diameter is positioned upstream (towards the source) of the ZP at 550 mm distance. The OSA with 10 µm in diameter was introduced in the optical scheme 6 mm downstream of the ZP. Figure 2 illustrates the modulation of the wave front acquired by raster scanning the first diffraction order with a photodiode detector shaped by a 10 µm diameter pinhole.

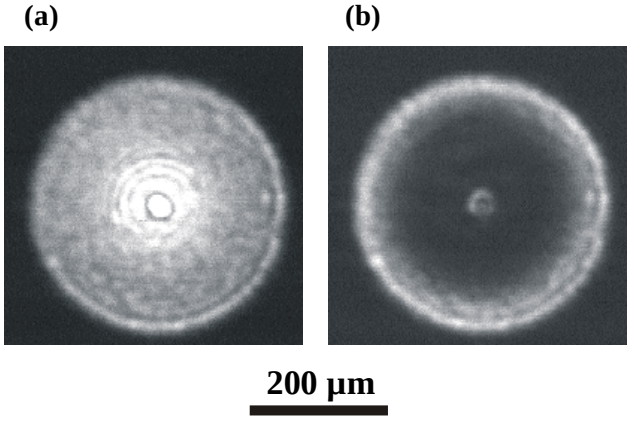

Fig. 2: First diffraction order of the microprobe forming ZP scanned by a photodiode shaped with a 10 µm pinhole. The images with 200x200 pixel and 2 µm x 2 µm pixel size were acquired with a dwell time of 50 ms/ px. (a) Raster scan without central stop with Fresnel diffraction fringes from the OSA in the central part overlapped to a speckle pattern resulting from X-ray source and ZP diffraction efficiency inhomogeneities. (b) Raster scan with central stop in the optical scheme.

#1552 - $15.00 US
Received August 09, 2002; Revised September 27, 2002

The detector was positioned 360 mm downstream of the back-focal plane leading to a 5 times magnification of the ZP pupil or a pupil diameter of 370 µm in the detector plane. The left image in Fig. 2 is a raster scan without the central stop and the diffraction from the OSA in the central and outermost part is overlapped to the speckle pattern resulting from variations in first order diffraction efficiency and X-ray source inhomogeneities. The right image in Fig. 2 is the corresponding raster scan with a 40 µm diameter central stop introduced 55cm upstream of the ZP. The central stop is made in 2 µm thick Au and has a residual transmission of 18 % at 6 keV.

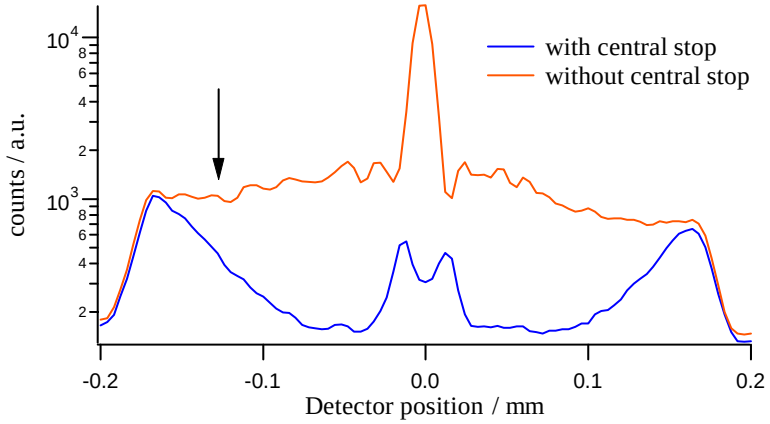

Fig. 3: Horizontal line scan through the center of the raster images in Fig. 2 without and with central stop. The line scan is dominated by the on-axis zero order light passing through the OSA, resulting in the central peak, which is surrounded by OSA diffraction. In the outer part Speckle pattern dominates. The convolution of diffraction from OSA and central stop results in a central double peak and a broad fringe slope in the outer part. The arrow indicates the detector position on this fringe slope.

3. Theoretical background

The origin of the contrast can be better understood by referring to previous investigations on the generation of phase contrast in the SEM (scanning electron microscope). Waddell and Chapman [13] give simple expressions of the optical transfer functions (OTF) of a scanning microscope, applicable to the real and imaginary part of the object transmission when the object modulation is weak. When the detector is in the object far field, the OTF applicable to the phase component is

$$F(\mathbf{k}) = P^*(-\mathbf{k}) \otimes [P(\mathbf{k})\, D(\mathbf{k})] - P(\mathbf{k}) \otimes [P^*(-\mathbf{k})\, D(-\mathbf{k})] \qquad (1)$$

where P(**k**) is the complex amplitude of the transmitted wave front (without object) in the detector plane and D(**k**) is the detector function (for a uniform detector, D(**k**) = 1 on the detector area and 0 outside). In the present case, the illumination scheme being symmetrical around the optical axis, P(**k**) is a real function. To simplify we also assume that the detector area is small enough that we can neglect the variation of P over the detector area – with respect to the convolution operator even an 50% amplitude variation has a limited effect. Then the OTF may be approximated as the odd part of $[P \otimes D_0](\mathbf{k}_0 - \mathbf{k})$ where D_0 is the detection pinhole function and $\mathbf{k_0}$ is its lateral offset. Similarly, the OTF applicable to the absorption component would be the even part of the same function.

#1552 - $15.00 US
Received August 09, 2002; Revised September 27, 2002

In the experiments we have used detector pinhole sizes of 10 and 50 µm. To get an idea of the actual phase OTF, we can use the measured profiles $P_0(\mathbf{k})$, given in figure 3, corresponding to the convolution by a pinhole of 10 µm size. The transfer function has in this case a simple expression:

$$F(\mathbf{k}) = P_0(\mathbf{k}_0 - \mathbf{k}) - P_0(\mathbf{k}_0 + \mathbf{k}) \qquad (2)$$

In figure 4 are represented the transfer function obtained in the two illumination cases of figure 3 with the detector offset indicated by the arrow on this figure. Only the cut in the direction of the detector offset k_0 is shown. Both OTF have an anti-symmetric behavior that is the signature of a differential contrast. However, they significantly depart from the linear transfer function corresponding to the derivation operator. When the central stop is present, the behavior is close to that of a DIC light microscope for the low frequencies with k values less than 0.23 pupil diameter unit (i.e. aperture angle $\theta < 0.23$ mrad or spatial frequencies $\nu < 1.15$ µm^{-1} for 6keV X-rays, λ=2Å), but the contrast is reversed at higher frequencies. This contrast inversion is due the direction of the intensity gradient of the illumination wavefront at the k_0 position. When the central stop is not present, there is no contrast inversion but the response to the low frequencies, $k < 0.15$ pupil diameter ($\nu < 0.75$ µm^{-1}), is very weak. The comparison of pictures 5 (b) and 5 (c) in the result section illustrate the effect of the missing low frequencies. In picture 5 (b), the rising and falling edges are equally marked by a brighter line, while in picture 5 (c) one is marked by a darker line and the other by a brighter line. This gives a better impression of relief and makes the image easier to interpret.

The OTF applicable to the absorption component of the object transmission is not zero in this detection scheme. Due to the parity properties of the transfer functions, the absorption OTF can be cancelled without changing the phase one, by subtracting the signal from two symmetrically placed detectors. This complication however is not really useful with high energy X-rays because the absorption signal is usually too weak produce an observable bright-field image of the object and because, most often, phase and absorption are strongly correlated.

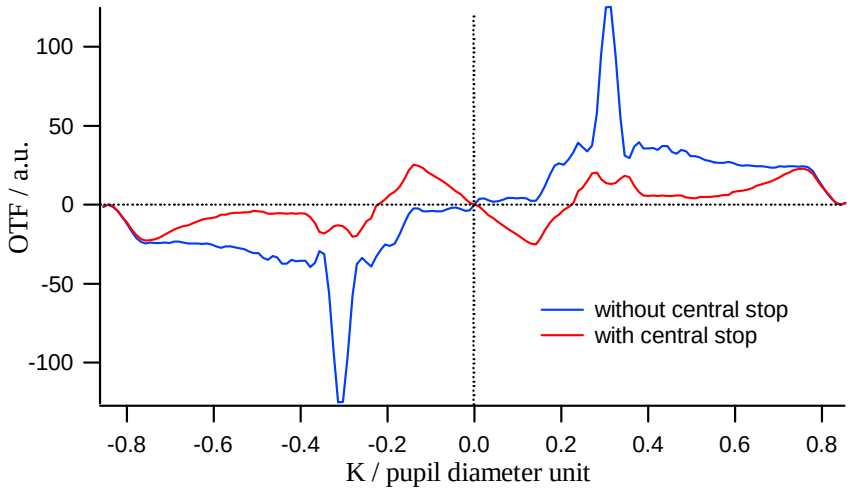

Fig. 4: Phase signal OTF of the DPC set-up using a small off-axis detector. Calculations have been performed with the measured pupil functions of figure 3; only the cut in the direction of the detector offset is shown. Red line: the wavefont is shaped by a central stop. Blue line: the central stop is taken out.

#1552 - $15.00 US Received August 09, 2002; Revised September 27, 2002

3. Results

The potential of this differential phase contrast technique for X-rays is demonstrated in the following X-ray images. Figure 4 compares the contrast of X-ray images of 2 μm thick PMMA grating structures at 6 keV photon energy. At this energy, PMMA has optical properties similar to biological matter: the real part of the refractive index (the phase shifting part revealed by DPC) is two orders of magnitude larger than the imaginary part (the absorbing part that is the only source of contrast in bright-field imaging). Actual values of PMMA refractive index ($n = 1-\delta - \iota\beta$) at 6 KeV, are: $\delta = 7.5 \times 10^{-6}$, $\beta = 3.0 \times 10^{-8}$, and the 2μm thick grating structures have a transmission of 99.6 %. Figure 5 (a) was acquired in absorption or bright-field contrast by removing the shaping aperture in front of the detector and integrating the signal. The structures can hardly be seen and the image contrast is far below 1 %. Figure 5 (b) was acquired without central stop, but with the detector shaped with a 10 μm pinhole aligned in the image plane as indicated in Fig.3. The slight increase in image contrast up to 3 % is correlated to the wave front modulation in the image plane by Speckle pattern and diffraction by the central stop. In Fig. 5 (c), the 40 μm central stop was introduced in the optical scheme and a tremendous increase of image contrast of 23 % is observed. Replacing the 10 μm pinhole shaping the detector by a 50 μm pinhole leads as shown in Fig. 5 (d) to better signal to noise ratio and as expected to an increase in spatial resolution. It has to be noted that the images were not processed and the horizontal intensity fluctuations are a result of low frequency source fluctuations during raster scanning. The 3D appearance or shadowing is similar to Nomarski interference contrast in visible light and due to the directionality of the amplitude slope of the transmitted wave front in the neighborhood of the detection pinhole

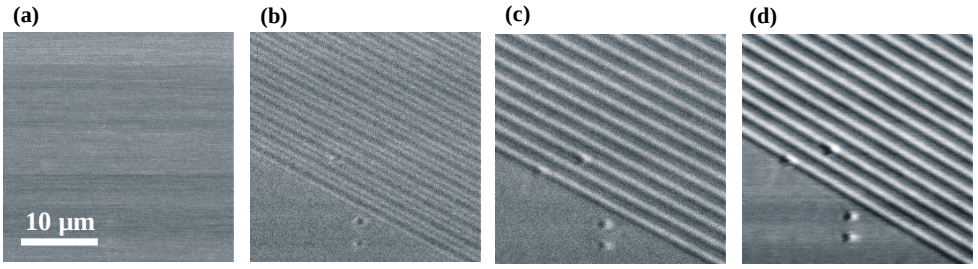

Fig. 5. Comparison of bright-field imaging with DPC X-ray imaging under different conditions. The X-ray images show 2 μm thick PMMA grating structures with a transmission of 99.6 % transmission at 6 keV photon energy. The acquisition time was in all cases 50 ms/ px. (a) is acquired in bright-field imaging mode without pinhole shaping the detector and integrating over the entire detector area. (b) DPC X-ray image with a 10 μm pinhole shaping the detector, but without central stop. (c) Is the corresponding DPC X-ray image with central stop introduced into the optical scheme. (d) DPC X-ray image, where the 10 μm pinhole in front of the detector was replaced by a 50 μm pinhole.

#1552 - $15.00 US Received August 09, 2002; Revised September 27, 2002

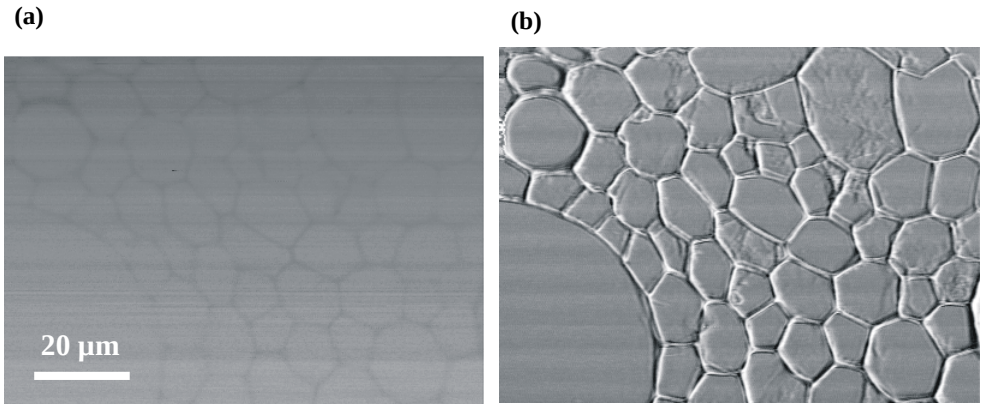

Fig. 6. Comparison of (a) bright-field imaging and (b) DPC imaging of cell membranes of maize plant cells. The acquisition time of the 400 x 300 pixel images was 50 ms/ px. A 50 µm pinhole was used to shape the detector.

The X-ray images in Figure 6 show a comparison of cells of a maize plant acquired in bright-field imaging mode (a) and X-ray DPC (b) with central stop and 50 µm pinhole shaping the detector. The almost transparent membrane structures are clearly visible in X-ray DPC mode.

4. Conclusion

We described a simple phase contrast technique to obtain high contrast images of transparent objects at X-ray wavelengths. Compared to other recently reported X-ray DPC techniques, this approach does not require any additional optical component into the microscope scheme. Since it depends upon the optical properties of a single, conventional zone plate optic, it allows to operate a zone plate based X-ray microscope at photon energies, spatial resolutions and imaging performances achieved in bright-field imaging. Easy switching between bright-field imaging and X-ray DPC imaging is possible by simply removing the shaping pinhole in front of the detector. In difference to the recently reported X-ray DIC (differential interference contrast) technique applying special diffractive optical elements for X-rays ('twin ZP'), this approach is limited to scanning type microscopes and can not be applied in full-field imaging type microscopes.

Since this X-ray DPC technique is strongly correlated to slope and extension of the intensity modulations of the illumination wave front, the performance of this technique can be improved by optimizing the position and diameter of the diffraction and detector shaping apertures. This will require pursue the theoretical investigations in order to better understand the convolution of the diffraction of the two apertures for an optimal wave front profile and determine the optimum position, shape and size of the detector elements.

Acknowledgement

We would like to thank gratefully the ESRF ID21 beamline staff for their outstanding support, especially Murielle Salomé, Barbara Fayard and Robert Baker. This work is supported by the European Community - Access to Research Infrastructure action of the Improving Human Potential Programme under contract HPRI-CT-2001-50024.

#1552 - $15.00 US Received August 09, 2002; Revised September 27, 2002